COMPDYN 2015
5th ECCOMAS Thematic Conference on
Computational Methods in Structural Dynamics and Earthquake Engineering
M. Papadrakakis, V. Papadopoulos, V. Plevris (eds.)
Crete Island, Greece, 25–27 May 2015

META-MODELING FOR CONSISTENT SEISMIC RESPONSE ANALYSIS

Muneo Hori[1,2], Seizo Tanaka[1], Tsuyoshi Ichimura[1], W.L.L. Wijerathne[1] and J.A.S.C. Jayasinghe[1]

[1]Earthquake Research Institute, The University of Tokyo, 1-1-1 Yayoi, Bunkyo, Tokyo 113-0032
e-mail: {hori,stanaka,ichimura,lalith,spoon}@eri.u-tokyo.ac.jp

[2]Advanced Institute for Computational Science, RIKEN, 7-1-26 Minatoshima Minamimachi, Chuo, Kobe, Hyogo 650-0047
e-mail: muneo.hori@riken.jp

Keywords: Continuum Mechanics, Structure Mechanics, Consistent Modeling, Lagrangian.

Abstract. *Depending on the numerical accuracy required, we can choose a simple mass spring system or a solid element model in carrying out structural seismic response analysis. The important issue is the consistency of the models, and meta-modeling proposed by the authors gives a solution to this issue. Presuming that continuum mechanics is the foundation of structural seismic response, for which a suitable Lagrangian is formulated, a model is constructed by making suitable mathematical approximations, and hence the model is consistent in the sense that it is used to solve the identical physical problem of estimating structural seismic responses. In this paper, we explain the basic concepts of meta-modeling and present numerical experiments of constructing consistent models for actual structures such as a large scale tunnel and a freeway bridge.*

1 INTRODUCTION

In earthquake engineering, the use of a structure element, such as truss, beam, plate, or shell is a usual practice; see, for instance, [8, 9]. It is rare that solid element analysis is made for a structure of complicated configuration, even though solid element analysis becomes much easier and less expensive due to the progress of computer hardware and software. While there are several reasons for rare use of solid element analysis, a major reason is that it is believed that the structure element analysis is able to make more accurate estimation, compared with the solid element analysis.

The authors are proposing a *meta-modeling* theory [1]. The essence of this theory is that there are structure mechanics modelings that are *consistent* with continuum mechanics modeling. Hence, the structure element analysis that stems from consistent structure mechanics modeling is mathematical approximation of the solid element analysis that corresponds to continuum mechanics modeling. That is, structure mechanics modeling solves the physical problem of continuum mechanics modeling by applying suitable approximation.

There is a trade-off relation between computational cost and numerical accuracy; see Table 1. According to meta-modeling, solid element analysis that uses a model of high fidelity is an extreme case of high accuracy and high cost. Structure element analysis ends up much less computational cost, with some loss of the numerical accuracy. A key issue here is that the same physical problem is solved; due to difference in mathematical approximation, the physical problem is converted to different mathematical problems. The meta-model theory clarifies this point, and it is the choice of a user whether he employs solid or structure element analysis considering the trade-off relation between the computational cost and the numerical accuracy of solving the same physical problem.

The content of this paper is as follows. First, the meta-modeling theory is briefly summarized in Section 2. As illustrative examples, we study lumped mass modeling and beam theory and present beam theory that is consistent with continuum modeling in Section 3. Numerical examples of applying meta-modeling to tunnel and highway networks are presented in Section 4. Concluding remarks are made at the end.

2 SUMMARY OF META-MODELING

We start from a Lagrangian of an elasticity body, V. For simplicity, we assume that the body is homogeneous and has isotropic elasticity tensor and density, denoted by $\mathbf{c}$ and ρ, respectively. Denoting velocity and strain by $\mathbf{v}$ and $\boldsymbol{\epsilon}$, respectively, we write the Lagrangian as

$$\mathcal{L}[\mathbf{v}, \boldsymbol{\epsilon}] = \int_V \frac{1}{2}\,\rho\mathbf{v}\cdot\mathbf{v} - \frac{1}{2}\boldsymbol{\epsilon} : \mathbf{c} : \boldsymbol{\epsilon}\,\mathrm{d}v, \tag{1}$$

where $\cdot$ and $:$ are the inner product and the second-order contraction. For displacement $\mathbf{u}$ which satisfies suitably prescribed boundary and initial conditions, we compute $\mathbf{v} = \dot{\mathbf{u}}$ and

Table 1: Trade-off relation between computational cost and numerical accuracy.

	soil-structure interaction	computation cost	data	distribution of accuracy
solid element	interface condition	large	material	uniform
structure element	special arraignment	small	structure component	high at measured point

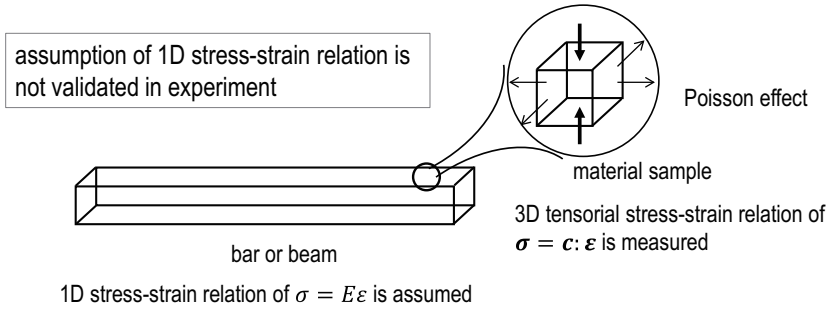

Figure 1: Assumption of one-dimensional stress-strain relation.

$\boldsymbol{\epsilon} = \mathrm{sym}\boldsymbol{\nabla}\mathbf{u}$ with $\dot{(.)}$ and $\boldsymbol{\nabla}(.)$ being temporal and gradient of $(.)$ and sym standing for the symmetric part of a second-order tensor.

Structure mechanics does not use the fourth-order tensor $\mathbf{c}$ as material property of V. It uses Young's modulus, E, instead. More specifically, structure mechanics employs a one-dimensional stress-strain relation expressed in terms of E. For instance, in the Cartesian coordinate of $\{x_1, x_2, x_3\}$, the normal stress and strain components in the x_1-direction are related as

$$\sigma_{11} = E\,\epsilon_{11},$$

rather than $\boldsymbol{\sigma} = \mathbf{c} : \boldsymbol{\epsilon}$ or

$$\sigma_{11} = c_{1111}\epsilon_{11} + \cdots = \frac{(1-\nu)E}{(1+\nu)(1-2\nu)}\epsilon_{11} + \cdots .,$$

where $\boldsymbol{\sigma}$ is stress tensor. While it is usually used, it is not understood that the assumption of the one-dimensional stress-strain relation is not validated in experiments, which assure the tensorial relation of $\boldsymbol{\epsilon}$ and $\boldsymbol{\sigma}$ via the fourth-order tensor $\mathbf{c}$; see Fig. 1.

Meta-modeling does not employ the one-dimensional stress-strain relation [1]. Instead, it modifies the Lagrangian as

$$\mathcal{L}^*[\mathbf{v}, \boldsymbol{\epsilon}, \boldsymbol{\sigma}] = \int_V \frac{1}{2}\rho\,\mathbf{v}\cdot\mathbf{v} - (\boldsymbol{\sigma} : \boldsymbol{\epsilon} - \frac{1}{2}\boldsymbol{\sigma} : \mathbf{c}^{-1} : \boldsymbol{\sigma})\,\mathrm{d}v. \tag{2}$$

where $\mathbf{c}^{-1}$ is the inverse fourth-order tensor of $\mathbf{c}$. It is readily shown that, if non-zero components of $\boldsymbol{\epsilon}$ and $\boldsymbol{\sigma}$ are ϵ_{11} and σ_{11} only, the second term in the integrand becomes $\sigma_{11}\epsilon_{11} - \frac{1}{2}\sigma_{11}^2/E$, and the variation with respect to σ_{11} is

$$\delta\left(\sigma_{11}\epsilon_{11} - \frac{1}{2}\frac{\sigma_{11}^2}{E}\right) = \frac{\delta\sigma_{11}}{E}(E\epsilon_{11} - \sigma_{11}).$$

As is seen, the one-dimensional stress strain relation is derived from the mathematical operation of taking variation. It is readily shown that $\mathcal{L}^*$ of Eq. (2) is equivalent with $\mathcal{L}$ of Eq. (1) in the sense that $\mathbf{u}$ that stationarizes $\mathcal{L}^*$ coincides with $\mathbf{u}$ for $\mathcal{L}$.

Meta-modeling leads to consistent modeling which solves the variational problem of $\mathcal{L}^*$. If no approximation is made for $\mathbf{u}$ (that produces $\mathbf{v}$ and $\boldsymbol{\epsilon}$) and $\boldsymbol{\sigma}$, it results in continuum mechanics modeling, and the governing equation for $\mathbf{u}$ is the wave equation, i.e.,

$$\rho\,\ddot{\mathbf{u}}(\mathbf{x}, t) - \boldsymbol{\nabla}\cdot(\mathbf{c} : \boldsymbol{\nabla}\mathbf{u}(\mathbf{x}, t)) = \mathbf{0}; \tag{3}$$

see, for instance, [4]. If certain approximations are made for $\mathbf{u}$ and $\mathbf{v}$, it results in a consistent modeling that solves the same variational problem of the Lagrangian using different partial differential equations.

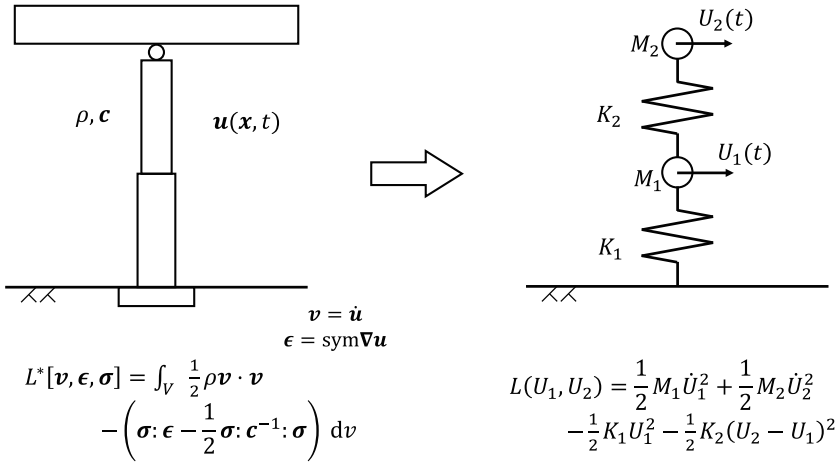

Figure 2: Schematic view of mass spring system consisting of two mass points.

3 EXAMPLES OF META-MODELING

In this section, we present two examples of applying the meta-modeling theory to make consistent modeling. They are modeling for mass spring system and modeling for beam theory.

3.1 Mass spring system

As the simplest case, we consider a mass spring system which consists of two mass points, as shown in Fig. 2. According to the meta-modeling theory, we consider an approximate displacement function of the following form:

$$\mathbf{u}(\mathbf{x},t) = \sum_{\alpha=1}^{2} U^{\alpha}(t)\boldsymbol{\phi}^{\alpha}(\mathbf{x}), \tag{4}$$

where U^{α} is a certain direction component of the α-th mass point and $\boldsymbol{\phi}^{\alpha}$ is displacement mode; by definition, a component of $\boldsymbol{\phi}^{\alpha}(\mathbf{x}^{\alpha})$ which corresponds to U^{α} takes on a value of 1, with $\mathbf{x}^{\alpha}$ being the location of the α-th mass point, and $\boldsymbol{\phi}^{\alpha}(\mathbf{x}^{\beta}) = \mathbf{0}$ for $\alpha \neq \beta$.

For simplicity, we substitute $\mathbf{u}$ of Eq. (4) into $\mathcal{L}$ of Eq. (1) rather than $\mathcal{L}^*$ of Eq. (2) which requires setting of $\boldsymbol{\sigma}$. We obtain

$$\mathcal{L} = \sum_{\alpha,\beta} \frac{1}{2} m^{\alpha\beta}\dot{U}^{\alpha}\dot{U}^{\beta} - \frac{1}{2}k^{\alpha\beta}U^{\alpha}U^{\beta}$$

where

$$m^{\alpha\beta} = \int_V \rho\,\boldsymbol{\phi}^{\alpha}\boldsymbol{\phi}^{\beta}\,\mathrm{d}v, \quad k^{\alpha\beta} = \int_V \boldsymbol{\nabla}\boldsymbol{\phi}^{\alpha} : \mathbf{c} : \boldsymbol{\nabla}\boldsymbol{\phi}^{\beta}\,\mathrm{d}v. \tag{5}$$

We choose $\{\mathbf{u}^{\alpha}\}$ so that some elements of $\{m^{\alpha\beta}\}$ and $\{k^{\alpha\beta}\}$ vanish and the above $\mathcal{L}$ becomes

$$\mathcal{L} = \frac{1}{2}M^1(\dot{U}^1)^2 + \frac{1}{2}M^2(\dot{U}^2)^2 - \frac{1}{2}K^1(U^1)^2 - \frac{1}{2}K^2(U^2 - U^1)^2. \tag{6}$$

As is seen, this $\mathcal{L}$ corresponds to a Lagrangian of the mass spring system shown in Fig. 2; M^1 and M^2 are the bottom and top masses, and K^1 and K^2 are the spring connecting the bottom mass to the ground and the top mass to the bottom mass, respectively.

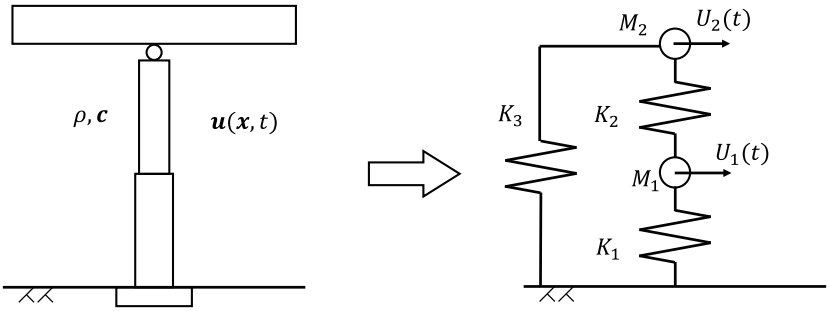

$$L^*[\boldsymbol{v},\boldsymbol{\epsilon},\boldsymbol{\sigma}] = \int_V \frac{1}{2}\rho\boldsymbol{v}\cdot\boldsymbol{v} - \left(\boldsymbol{\sigma}:\boldsymbol{\epsilon} - \frac{1}{2}\boldsymbol{\sigma}:\boldsymbol{c}^{-1}:\boldsymbol{\sigma}\right) \mathrm{d}v \qquad L(U_1,U_2) = \frac{1}{2}M_1\dot{U}_1^2 + \frac{1}{2}M_2\dot{U}_2^2 - \frac{1}{2}K_1U_1^2 - \frac{1}{2}K_2(U_2-U_1)^2 - \frac{1}{2}K_3U_2^2$$

Figure 3: Schematic view of consistent mass spring system consisting of two mass points.

It is easily seen that in order to derive $\mathcal{L}$ of Eq. (6), $\{\boldsymbol{\phi}^\alpha\}$ must satisfy

$$\int \rho\,\boldsymbol{\phi}^1\cdot\boldsymbol{\phi}^2\,\mathrm{d}v = 0, \quad \int (\boldsymbol{\nabla}\boldsymbol{\phi}^1 + \boldsymbol{\nabla}\boldsymbol{\phi}^2) : \mathbf{c} : \boldsymbol{\nabla}\boldsymbol{\phi}^2, \mathrm{d}v = 0.$$

Choosing $\{\boldsymbol{\phi}^\alpha\}$ that satisfy the first condition is relatively easy, compared with choosing $\{\boldsymbol{\phi}^\alpha\}$ that satisfy the second condition.

It is of interest to use the first two dynamic modes of V, denoted by $\{\boldsymbol{\psi}^\alpha\}$ with natural frequency $\{\omega^\alpha\}$ ($\alpha = 1$, 2). By definition, $\boldsymbol{\psi}^\alpha$ and ω^α satisfy

$$\rho\,(\omega^\alpha)^2\boldsymbol{\psi}^\alpha + \boldsymbol{\nabla}\cdot(\mathbf{c}:\boldsymbol{\nabla}\boldsymbol{\psi}^\alpha) = \mathbf{0},$$

and $\int \rho\boldsymbol{\psi}^\alpha\cdot\boldsymbol{\psi}^\beta\,\mathrm{d}v = 0$ and $\int \boldsymbol{\nabla}\boldsymbol{\psi}^\alpha : \mathbf{c} : \boldsymbol{\nabla}\boldsymbol{\psi}^\beta\,\mathrm{d}v = 0$ for $\omega^\alpha \neq \omega^\beta$. As is seen, $\{\boldsymbol{\psi}^\alpha\}$ decouple the kinematic energy but do not decouple the strain energy. That is, if $\{\boldsymbol{\psi}^\alpha\}$ are used for $\{\boldsymbol{\phi}^\alpha\}$ of Eq. (4), the Lagrangian becomes

$$\mathcal{L} = \frac{1}{2}M^1(\dot{U}^1)^2 + \frac{1}{2}M^2(\dot{U}^2)^2 - \frac{1}{2}K^1(U^1)^2 - \frac{1}{2}K^2(U^2-U^1)^2 - \frac{1}{2}K^3(U^2)^2. \tag{7}$$

Figure 3 shows a spring system which correspond to the above Lagrangian. This system has a third spring, denoted by K^3, that connects the top mass (M^2) to the ground. This spring is essential to make the system consistent so that the natural frequency coincides with that of the continuum. It should be noted that $\{\boldsymbol{\phi}^\alpha\}$ are set to satisfy the condition that a component of $\boldsymbol{\phi}^\alpha(\mathbf{x}^\alpha)$ which correspond to U^α is 1, but that they do not have to satisfy $\boldsymbol{\phi}^\alpha(\mathbf{x}^\beta) = \mathbf{0}$ for $\alpha \neq \beta$.

3.2 Beam theory

According to the meta-modeling theory, a governing equation of beam theory is derived from $\mathcal{L}^*$ of Eq. (2), by using $\{\mathbf{u}, \boldsymbol{\sigma}\}$ of the following non-zero components:

$$u_1 = -z\,w'(x,t), \quad u_3 = w(x,t), \quad \sigma_{11} = z\,s(x,t). \tag{8}$$

Here, the x_1- and x_3-axes are the longitudinal and (bending) transverse directions, and x and z are used instead of x_1 and x_3.

Since $\mathcal{L}^*$ becomes a functional of w and s, the variation of $\mathcal{L}^*$ with respect to these functions is

$$\delta\mathcal{L} = \int \delta w\left(\rho(\ddot{w}^2 - z^2\ddot{w}'' + z^2s''\right)\delta s z^2(\frac{s}{E} + w'')\,\mathrm{d}x\mathrm{d}y\mathrm{d}z. \tag{9}$$

Recall that $\mathbf{c}$ is assumed to be homogeneous and isotropic; Young's modulus and Poisson's ratio are E and ν. It thus yields $s = -E\,w''$ and

$$\rho\,A\,\ddot{w}^2 - \rho\,I\,\ddot{w}'' - (E\,I\,w'')'' = 0, \tag{10}$$

where $A = \int \mathrm{d}z\,\mathrm{d}y$ and $I = \int z^2\,\mathrm{d}z\,\mathrm{d}y$. As is seen, this equation for w coincides with the governing equation of Rayleigh beam theory; at quasi-static state, Eq. (10) yields the governing equation of Bernoui Euler beam theory, too.

A beam element solution is now regarded as an approximate numerical solution of solving the variational problem of $\mathcal{L}^*$. A beam element solution which is *closest* to a solid element solution is determined by minimizing a suitable distance in the function space of $\{\mathbf{u}, \boldsymbol{\sigma}\}$. For instance, when a solid element solution $\{\overline{\mathbf{u}}, \overline{\boldsymbol{\sigma}}\}$ is given, we measure the distance of a beam element solution given by w as follows:

$$N(w) = \frac{1}{|\overline{\mathbf{u}}|^2}\int (w - \overline{u}_1)^2 + (-zw' - \overline{u}_3)^2\,\mathrm{d}v + \frac{1}{|\overline{\boldsymbol{\sigma}}|^2}\int (\overline{\sigma}_{11} - zEw'')^2\mathrm{d}v, \tag{11}$$

where $||^2$ is the L2 norm of $\overline{\mathbf{u}}$ and $\overline{\boldsymbol{\sigma}}$; $\frac{1}{|\overline{\mathbf{u}}|^2}$ and $\frac{1}{|\overline{\boldsymbol{\sigma}}|^2}$ are necessary so that N does not have physical dimension of length nor stress.

It is a usual practice of the beam element analysis that a rotation function, θ, is introduced besides for deflection, w. This θ provides $u_1 = -z\theta$ and $\sigma_{11} = -Ez\theta'$, since it is defined as $\theta = -w'$. In numerical computation, θ is discretized separately from w in order to obtain a more accurate solution. Hence, w' is replaced by θ in N of Eq. (11) when θ is used in the beam element analysis.

The conversion from the solid element solution to a beam element solution is readily made by minimizing N. In discretized index form, $\overline{\mathbf{u}}$ and $\overline{\boldsymbol{\sigma}}$ are expressed as

$$\overline{\mathbf{u}} = \sum_\alpha \overline{\mathbf{u}}^\alpha \phi^\alpha(\mathbf{x}), \quad \overline{\boldsymbol{\sigma}} = \sum_\alpha \mathbf{c} : (\overline{\mathbf{u}}^\alpha \otimes \boldsymbol{\nabla}\phi^\alpha(\mathbf{x})), \tag{12}$$

where $\mathbf{u}^\alpha$ and ϕ^α are the α-th nodal displacement and shape function, respectively. Similarly, w and θ are expressed as

$$w = \sum_\beta w^\beta \psi^\beta(x), \quad \theta = \sum_\beta \theta^\beta \psi^\beta(x), \tag{13}$$

where w^β, θ^β and ψ^β are the β-th nodal displacement, rotation and shape function, respectively. In order to minimize N, $\{w^\beta\}$ and $\{\theta^\beta\}$ satisfy

$$\sum_\beta A^{\gamma\beta} w^\beta + \sum_\alpha B^{\gamma\alpha}\overline{u}_3^\alpha = 0, \quad \sum_\beta C^{\gamma\beta}\theta^\beta - \sum_\alpha D^{\gamma\alpha}\overline{u}_i^\alpha = 0, \tag{14}$$

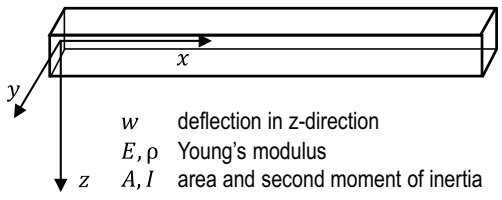

Figure 4: Schematic view of beam and coordinate system.

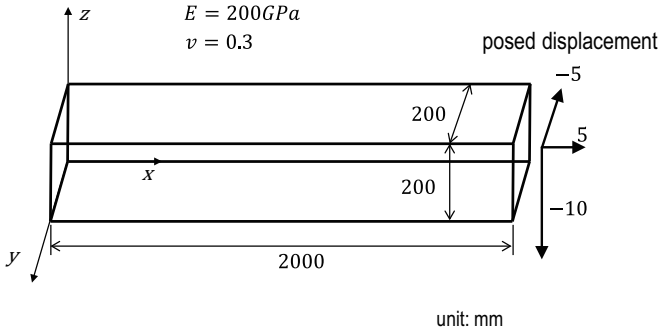

Figure 5: Schematic view of cantilever beam.

for $\gamma = 1, 2, \cdots$, where

$$A^{\gamma\beta} = (\psi^\gamma \psi^\alpha), \quad B^{\gamma\alpha} = (\psi^\gamma \phi^\alpha), \quad C^{\gamma\beta} = (z^2 \psi^\gamma \psi^\beta) + \frac{(\overline{\mathbf{u}} : \overline{\mathbf{u}})}{(\overline{\boldsymbol{\sigma}} : \overline{\boldsymbol{\sigma}})} E^2((\psi^{\gamma\prime}(\psi^{\beta\prime}),$$
$$D_i^{\gamma\alpha} = \delta_{3i}(z\psi^\gamma \phi^\alpha) + \frac{(\overline{\mathbf{u}} : \overline{\mathbf{u}})}{(\overline{\boldsymbol{\sigma}} : \overline{\boldsymbol{\sigma}})}(E\psi^\gamma c_{33ij} \frac{\partial \phi^\alpha}{\partial x_j}). \tag{15}$$

Here, for simplicity, $()$ is used to denote the volume integration taken over V, and summation convention is employed (repeated indices are summed).

4 NUMERICAL EXPERIMENTS FOR CONSISTENT MODELS

4.1 Cantilever beam

Biaxial bending in beam or column is encountered in structural analysis [5]FF. Prediction of bidirectional bending made by ordinary methods is not a simple task due to coupling of biaxial bending with axial force; the ordinary methods employs interpolation and curve fitting of element stress (or nodal stress that is computed from element stress) in order to compute biaxial bending moment. The meta-modeling theory is readily able to decouple biaxial bending moment without introducing any assumption, since it uses genuinely mathematical approximation of functions. In this subsection, we examine the capability of the meta-modeling theory of handling the de-coupling of biaxial bending moment.

A cantilever with uniform square (200 $\times$ 200 mm) cross section is used in the present numerical experiment; see Fig. 5 for the problem setting of the cantilever. Three boundary conditions of displacement are posed at one end, while the other end is clamped. Sufficiently fine mesh is used for both the solid and beam element models. This is essential for the numerical model that is used in the meta-modeling, in order to remove (or minimize) numerical errors caused by coarse meshing.

A solid element solution is converted to a beam element solution, according to the procedures present in the preceding section. The cross-section forces which are computed by the converted beam element solution are shown in Fig. 6. For comparison, the cross sectional force which are computed by the conventional method that uses interpolation and curve fitting of element stress are shown in the figure, too. As is seen, there are some differences in the converted forces and the estimated ones. However, the difference is not significant, suggesting that the cross sectional force computed by the converted beam element solution is sufficiently accurate.

It should be emphasized that de-coupling of the biaxial bending moment is successfully made in the proposed conversion method that is based on the meta-modeling theory. The converted

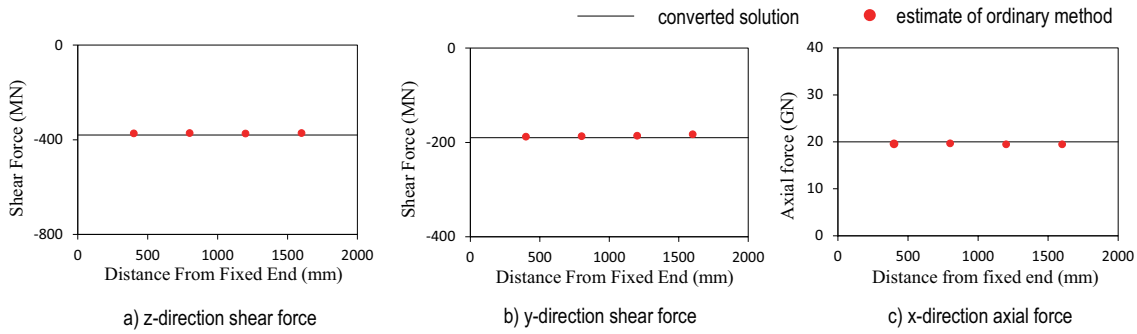

Figure 6: Distribution of cross-sectional force of cantilever computed by converted beam element solution.

beam element solution has a set of displacement and cross-sectional force. The conventional method which calculates cross-sectional force from element stress does not produce such a set. Moreover, interpolation and curve fitting of element stress is laborious when cross sectional force and moment are computed at every cross section. The proposed conversion method is much simpler, since it casts a solid element solution to a beam element solution just by solving Eq. (14) so that the closest beam element solution is found.

4.2 Tunnel structure

A tunnel needs a ramp tunnel which connects the main tunnel to the ground level. By this nature, the ramp tunnel has a complicated configuration and the resulting seismic response ought to be complicated; it often passes through several soil layers of different wave velocities. Therefore, two-dimensional analysis of cross-section has limited accuracy in estimating such complicated responses. Three-dimensional solid element analysis is needed if the seismic response has to be evaluated at highest accuracy [2, 3]. For the purpose of design, cross sectional forces and moment are of primary importance, and hence the results of the three-dimensional solid element analysis must be converted to cross sectional force and moment, in the same manner as shown in the preceding subsection.

A solid element model of a main tunnel connected by a ramp tunnel is used in the present numerical experiment; see Fig. 7 for a schematic view of the tunnel. It should be mentioned that this model is a part of a solid element model that is used for large-scale numerical computation of the main tunnel, the length of which is longer than 2,000 m. A targeting frequency range of the present model is 0 to 6 Hz, and suitably fine meshing is made for the model. Longitudinal ground motion is input to the tunnel; see Fig. 8 for the wave form of the input ground motion.

For simplicity, we convert a solid element solution at an instant at when displacement takes on a maximum value. It is indeed laborious to convert a time series of the solid element solution to that of the beam element solution. However, this conversion is much easier than computing cross sectional force and moment by the conventional method that uses interpolation and curve fitting of element stress. Spatial distribution of three cross sectional forces which are computed from the converted beam element solution are presented in Figs. 9 and 10; the latter shows rapid change in the cross sectional forces along the longitudinal direction of the tunnel. At three cross sections, the forces that are computed by the converted beam element solution are compared with those computed by the ordinary method; see Table 2 for the values of the cross sectional forces.

As is seen in Fig. 10, the main part of the tunnel behaves like rod rather than beam, since the axial force is dominant in the cross sectional forces and the shear force and bending moment

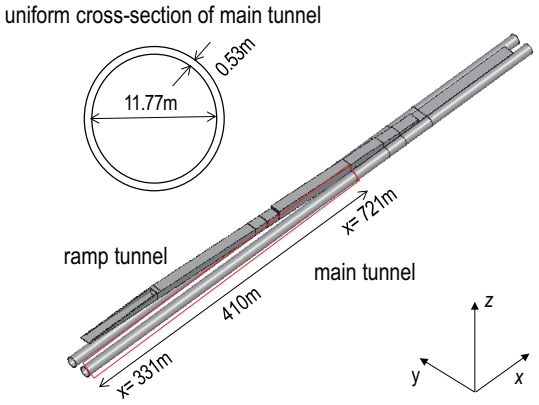

Figure 7: Schematic view of large scale tunnel with ramp tunnel.

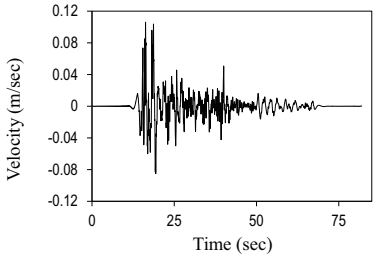

Figure 8: Input ground motion of tunnel.

Table 2: Comparison of cross sectional force of tunnel computed by converted beam element solution.

a) z-direction shear force

location	proposed	ordinary
400	-109.21	-105.22
500	-23.15	-30.22
600	-36.88	-32.24

b) y-direction shear force

location	proposed	ordinary
400	59.66	65.25
500	1.27	3.21
600	1.45	3.25

is small. It is also easily seen that the distribution of the cross sectional forces is not uniform; concentration is observed between 400 m and 500 m along the tunnel longitudinal direction. Choosing a part of the tunnel in which the cross sectional forces are concentrated is easily found. The location of such concentration of the cross sectional force could be different from that of stress. For the purpose of design, it is surely better to use the cross sectional forces if they are easily computed.

Difference in computing the cross sectional force between the present conversion method and the ordinary method is not negligible. Larger relative difference is found for the shear force compared with the axial force. But this is probably because the shear force is smaller than the axial force. These results suggest that the numerical accuracy of computing the cross sectional force from the converted beam element solution is sufficiently high, just like the cantilever of the preceding subsection. We can see a potential usefulness of the conversion method that is based on the meta-modeling theory, since it accurately estimates cross sectional forces that are associated with the converted displacement of the beam theory.

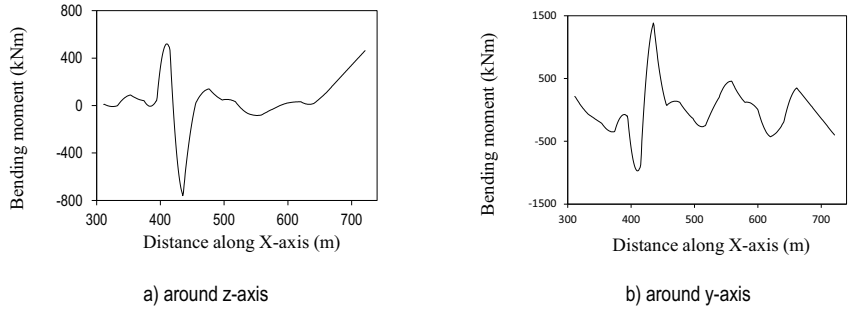

Figure 9: Distribution of cross-sectional force of tunnel computed by converted beam element solution.

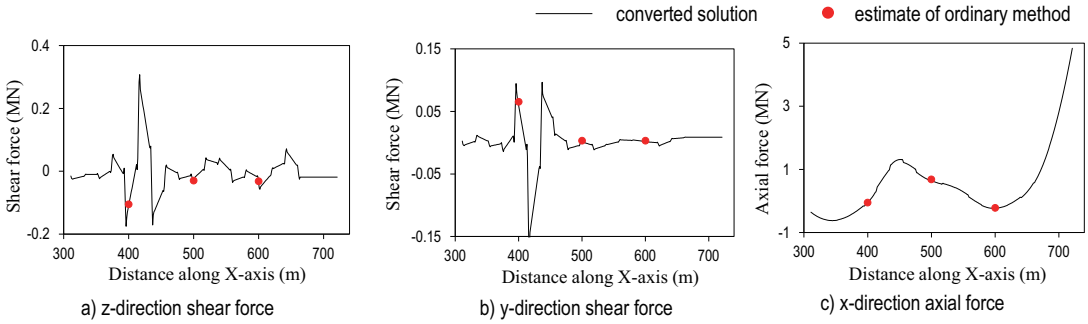

Figure 10: Detailed distribution of cross-sectional force of tunnel computed by converted beam element solution.

4.3 Freeway bridge structure

A freeway bridge which consists of a few pier and a deck is large in scale and complicated in configuration, and it is another target of seismic response analysis that uses the three-dimensional solid element analysis. Modeling connection between the pier and the deck is not straightforward since shoes and bearings that have distinct friction characteristic are used there. Indeed, there are cases when analysis models have natural frequencies different from the observation. The meta-modeling theory could help us to construct a solid element model of high fidelity by gradually increasing the complexity of consistent models.

As an example, we consider a freeway bridge as shown in Fig. 11; it has a curved deck supported by fourteen piers. The material properties are summarized in Table 3. Beside for the deck being curved, the height of the piers is not uniform and each pier has its own configuration. For simplicity, however, we assume that all the piers share the identical cross section, as shown in Fig. 12, while the height of the piers is different.

According to the meta-modeling theory, we construct a mass spring system for each pier; the system consists of one mass and one spring. The mass and stiffness of each pier are presented in Fig. 13. And the natural frequency of the mass spring system of each pier is summarized in

Table 3: Material properties of freeway bridge.

density of pier (concrete)	$2400kg/m^3$
density of deck (steel)	$7800kg/m^3$
Young's modulus (concrete)	$25GPa$
Young's modulus (steel)	$200GPa$
damping ratio (concrete)	5%

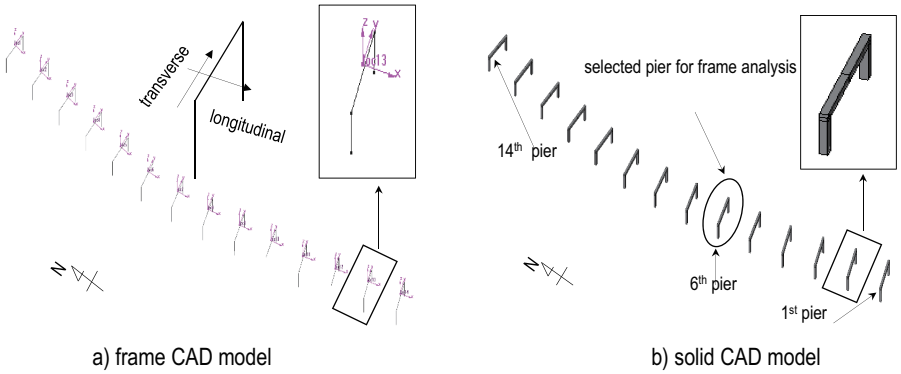

Figure 11: Schematic view of freeway bridge.

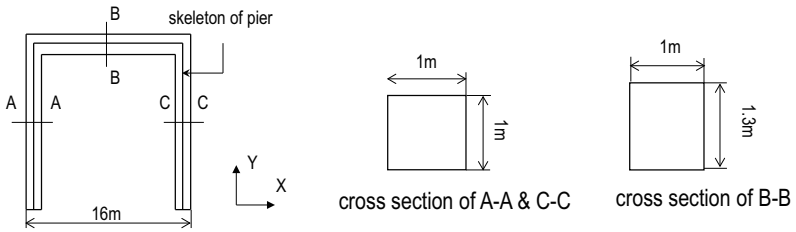

Figure 12: Cross section of freeway bridge.

Table 4: Comparison of natural frequency of freeway bridge computed by converted beam element solution.

	transverse (Hz)	longitudinal (Hz)
lumped mass	3.426	3.426
frame	3.420	3.421

Table. 4.

For some piers, the maximum displacement of the mass spring system is compared with that of the frame model; see, for intance, [6, 9, 11, 12] for the comparison of the seismic response of bridge piers. The frame model is made by manual work, while the mass spring system is automatically constructed according to a given data of the freeway bridge; the mass spring system is much simpler than the frame model and hence we can make such automated model construction. While there are some differences in the natural frequency, they are not significant; see Table 4. This suggests that, for the natural frequency of the first mode, the mass spring system that is constructed by the meta-modeling theory is sufficiently accurate.

We compute seismic response of the piers of the free bridge using the mass spring system. Input ground motion is shown in Fig. 15. For comparison, we carry out the seismic response analysis using the frame model. The difference in the displacement response of the two models is presented in Fig. 16.

As is seen in Fig. 16, there are some difference in the response. This difference is inevitable since even the natural frequency of the mass spring system is different from that of the frame model; see Table 4. However, this difference is not significant since the peak displacement reaches a few ten centimeter. Again, this suggests high accuracy of the consistent mass spring system in computing the seismic response analysis.

Small difference in the seismic response is partial due to the nature of input ground motion which does not have large contribution of the higher modes of the bridge piers. It is inevitable

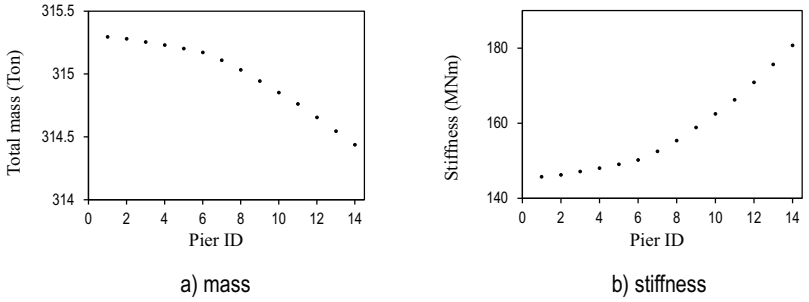

Figure 13: Mass and stiffness of mass spring system for bridge piers.

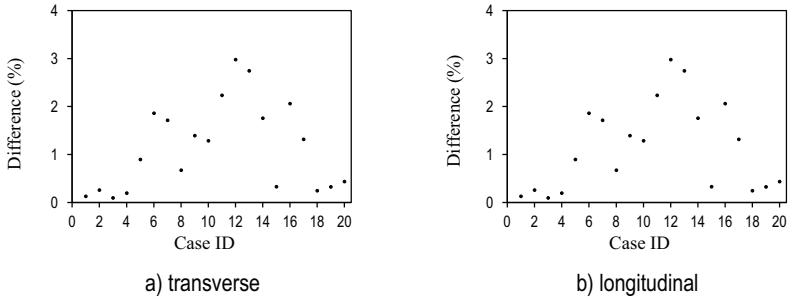

Figure 14: Maximum displacement of freeway bridge computed by converted beam element solution.

for a simple mass spring system to fail computing higher modes accurately. A simple solution to overcome this shortcoming of the mass spring system is to use a more complicated mass spring system which consists of a few masses and springs. Consistency is surely required for such a mass spring system which may need additional springs; compare Fig.3 with Fig. 2.

5 CONCLUDING REMARKS

This paper presents the meta-modeling theory and its application, in order to construct a set of consistent models for structure seismic response analysis. The consistency of modeling is that it solves the same variational problem of continuum mechanics by using different mathematical approximation. Consistent mass spring system and beam theory are explained. Numerical experiments demonstrate that for actual structures, this theory is applicable to construct a set of consistent models.

The present numerical experiments use linear analysis only. It is surely necessary to study the material and kinematic non-linearity, in applying the meta-modeling theory to construct consistent non-linear models. The key issue of this study is to find a Lagrangian for the non-linear case.

REFERENCES

[1] M. Hori, W.L.L. Wijerathne, T. Ichimura, S. Tanaka, Meta-modeling for constructing model consistent with continuum mechanics, *Journal of Stuctural Mechanics and Earthquake Engineering*, Vol. 9, No. 4, 2014.

[2] H. Dobashi, T. Hatsuku, T. Ichimura, M. Hori, T. Yamada, N. Ohbo, M. Moriguchi, H. Itami, Full 3d seismic response analysis of underground ramp tunnel structure using large-

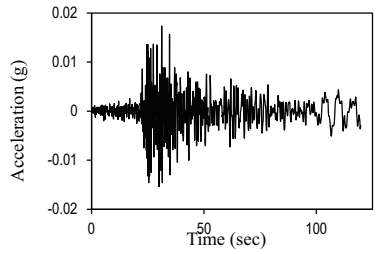

Figure 15: Input ground motion of freeway bridge.

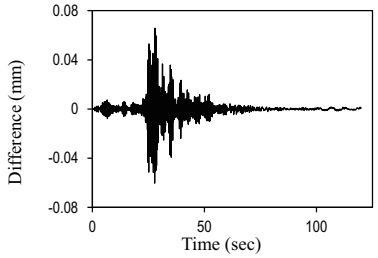

Figure 16: Difference in displacement response of freeway bridge computed by converted beam element solution.

scale numerical computation, *The 14th World Conference on Earthquake Engineering october*, Beijing, China, August, 2008.

[3] H. Dobashi, Y. Terashima, M. Hori, T. Ichimura, N. Ohbo, T. Yamada, T. Obara, Seismic performance analysis of underground ramp tunnel structure using 3-D massive numerical computation, *III ECCOMAS Thematic Conference on Computational Methods in Structural Dynamics and Earthquake Engineering*, Corfu, Greece, May, 2011.

[4] J. F. Doyle, *Wave Propagation in Structures*, Mechanical engineering series, 2nd edition, pp. 43–73, 1997.

[5] G. Li, J. Li, A tapered Timoshenko-Euler beam element for analysis of steel portal frames, *Journal of construc-tional steel research*, Vol. 58, No. 12, pp. 1531–1544, 2002.

[6] C. K. Wang, Stability of rigid frames with nonuniform members, *Journal of Structural Division*, Vol. 93, No. 1, pp. 275–294, 1967.

[7] H. V. S. G. Rao, Closed form series solutions of boundary value problems with variable properties, *Computers & Structures*, Vol. 23, No. 2, pp. 2110–215, 1986.

[8] A. K. Chopra, *Dynamics of Structures*, Prentice Hall Inter-national, 2nd edition, pp. 305–343, 2000.

[9] R. W. Clough, J. Penzien, *Dynamics of Structures*, McGraw-Hill International, 2nd edition, pp. 133–160, 2000.

[10] B. Jang, R. T. Chin, Analysis of Thinning Algorithms Using Mathematical Morphology, *Transactions on Pattern Analysis and Machine Intelligence*, Vol. 12, No. 6, 1990.

[11] M. J. Kowalsky, Deformation limit states for circular reinforced concrete bridge columns, *Journal of Structural Engineering*, Vol. 126, No. 8, 2000.

[12] M. J. Kowalsky, M. J. N. Priestley, G. A. Macrae, Displacement-based design of RC bridge columns in seismic regions, *Earthquake Engineering And Structural Dynamics*, Vol. 24, pp. 1623–1643, 1995.